Profiles of Raindrop Size Distributions as Retrieved by Microrain Radars

GERHARD PETERS AND BERND FISCHER

Meteorologisches Institut, Universität Hamburg, Hamburg, Germany

HANS MÜNSTER

Max-Planck-Institut für Meteorologie, Hamburg, Germany

MARCO CLEMENS

Institut für Meereskunde-GEOMAR, Kiel, Germany

ANDREAS WAGNER

Deutscher Wetterdienst, Hohenpeissenberg, Germany

(Manuscript received 16 October 2004, in final form 7 June 2005)

ABSTRACT

Data of vertically pointing microrain radars (MRRs), located at various sites around the Baltic Sea, were analyzed for a period of several years. From the Doppler spectra profiles of drop size distributions (DSDs) are obtained. A significant height dependence of the shape of the DSDs—and thus of the Z–R relations—is observed at high rain rates. This implies, for the considered sites, that ground-based Z–R relations lead to underestimation of high rain rates by weather radars.

1. Introduction

Radar precipitation measurements are made at increasing heights with an increasing range resulting from the earth's curvature. Because measurements aloft do not necessarily represent surface conditions of precipitation [often referred to as vertical profile of reflectivity (VPR)] various schemes have been devised in past decades to minimize the radar data's bias of precipitation. A review of adjustment methods based on gauge data and other auxiliary information can be found in Koistinen and Michelson (2002). While the effectiveness of these adjustment schemes is obvious for long-term (12 h or more) accumulation products, the usefulness of high-resolution radar data as needed, for example, for local-scale flood-warning purposes is still under discussion (Einfalt et al. 2004).

Here we focus on a feature of the VPR, which was not considered so far: while significant gradients of radar reflectivity are well known in and above the melting layer, constant reflectivity is generally assumed between the surface and the melting layer. We will report measurements of high-resolution profiles obtained with vertically pointing Doppler radars showing a significant shape transformation of drop size distributions, and thus of the Z–R-relation, on the fall path *below* the melting layer in the case of strong rain rates ($\geq$20 mm h^{-1}). Because rain events with such strong intensities do not occur often and are generally short lived, the related characteristic structure does not show up in mean VPRs containing all rain events. Therefore, we think that our observations are not in contrast to existing knowledge of VPRs, but are a consequence of the stratification of the data according to rain rates and the high spatial and temporal resolution of our measurements.

Motivated by surprisingly good agreement between radar reflectivities of a vertically pointing K-band microrain radar (MRR) and a C-band weather radar (Wagner et al. 2003; Peters et al. 2002), we resumed the suggestion of Atlas et al. (1973), who used Doppler

Corresponding author address: Gerhard Peters, Meteorologisches Institut, Universität Hamburg, Bundesstrasse 55, D20146 Hamburg, Germany.
E-mail: peters@miraculix.dkrz.de

radar at vertical incidence to derive information on the DSD via the relation between terminal fall velocity and drop size. No areal coverage is possible in this way, but the vertical structure of precipitation can be studied in detail. In addition, the implications inherent in the conversion of disdrometer flux data to DSDs Jameson and Kostinski (2001a) are avoided.

Datasets comprising several years, obtained with vertically pointing MRRs at three sites around the Baltic Sea, were analyzed. A map of the radar sites is shown in Fig. 1. The geographic radar positions, the analyzed periods, and pertinent operating parameters are given in Table 1.

To avoid the ice phase we restricted the data analysis presented here to the lower 1500 m during summer seasons.

The Doppler spectra, obtained at vertical incidence, reflect the fall velocity distribution of hydrometeors and can be converted into DSDs under the assumption of zero vertical wind. The last assumption is certainly not generally justified and may cause strong errors of individual DSDs and corresponding rain parameters derived there from. Nevertheless, the error analysis, discussed in appendix A, supports our confidence that the observed mean vertical structures of rain parameters actually reflect microphysical processes rather than are merely artifacts of the retrieval process.

Because there is no need for a parameterization of DSDs in this context, we preferred to use the DSDs directly as retrieved line by line from the Doppler spectra in order to derive the rain parameters and parameter-free Z–R relations as functions of measuring height.

Rain-rate profiles R obtained in this way are compared with profiles R_Z that would be obtained by using some conventional height-independent Z–R relation. For the latter a commonly used power law $Z = aR^b$ was chosen.

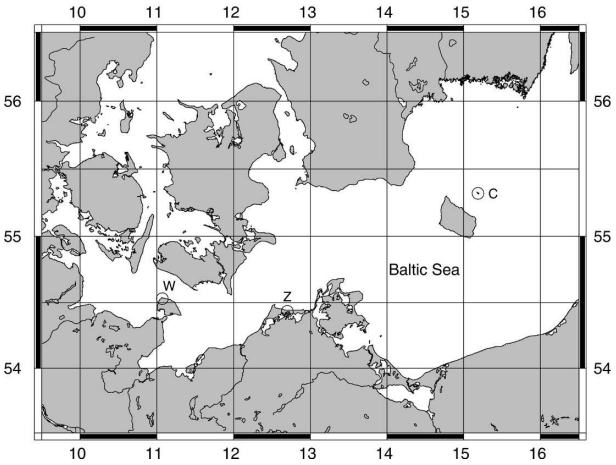

FIG. 1. Map of measuring sites: C = Christiansoe, W = Westermarkelsdorf, and Z = Zingst.

The aim of this paper is to show the different *height dependence* of rain rates derived in both ways, expressed by R/R_Z versus measuring height. Therefore, the actual choice of a reference Z–R relation and the agreement between R and R_Z at a particular height are of second priority.

After a brief description of the characteristics of the microrain radar in section 2 and the main steps of data processing in section 3, the results are presented in section 4.

In accordance with the admonition of Jameson and Kostinski (2001a) concerning the dependence of microphysical parameters on the observing method, the principle of the measurement and the retrieval algorithms including various corrections and error estimates are discussed in more detail in appendix A. Because the focus of this paper is to ascertain *mean* properties and structures of rain parameters, appendix B is devoted to potential pitfalls of averaging data with nonnormal distributions. The effect of turbulence on the width of averaged spectra and the dependence on the averaging procedure (arithmetic versus harmonic) is discussed in appendix C.

2. The microrain radar

The main characteristics of the MRR (METEK GmbH) are summarized in Table 2. The principle of frequency-modulated (FM)-continuous wave (CW) Doppler radar for volume filling targets has been described by Strauch (1971). The advantage of this type of radar is the small required transmitter power for a given radar sensitivity. Usually FM-CW radars need separated transmitting and receiving antennas. Thanks to the small transmit power (50 mW) of the MRR, a common antenna can be used here, so that no beam overlap problems need to be considered.

The database, analyzed in this study, consists of Doppler spectra $\eta(f)$, recorded at the various radar sites for periods up to 3 yr; $\eta(f)$ is the spectral volume backscattering cross section (m^{-1} s) at the Doppler shift f (s^{-1}). From these Doppler spectra the following microphysical parameters were retrieved: 1) drop size distribution $N(D)$ is the spectral number density (m^{-4}), 2) rain attenuation coefficient κ_r (m^{-1}) is related to the two-way attenuation $l(z)$ by

$$l(z) = \exp\left[-\int_0^z 2\kappa_r(z')\, dz' \right],$$

TABLE 1. MRR positions, analyzed periods, and operating parameters.

Position	Analyzed periods (1 May–30 Sep)	Time resolution (s)	Height resolution (m)	Height range (m)
Zingst: 54°26′N, 12°42′E	2000–02	60	100	300–3000
Westermarkelsdorf: 54°35′N, 11°06′E	2002–03	10	35	105–1050
Christiansoe: 55°19′N, 15°10′E	2000	60	100	300–3000

with height of the scattering volume z, 3) radar reflectivity factor

$$Z = \int_0^\infty N(D)D^6\,dD$$

($\mathrm{mm^6\ m^{-3}}$), 4) equivalent radar reflectivity factor

$$Z_e = \int_{-\infty}^{+\infty} \eta(f)\,df/A,$$

where A is a constant and Z and Z_e are identical in the Rayleigh approximation $D \ll$ radar wavelength λ, 5) liquid water content

$$\mathrm{LWC} = \rho_w(\pi/6)\int_0^\infty N(D)D^3\,dD$$

($\mathrm{g\ m^{-3}}$), with density of water ρ_w, 6) rain rate

$$R = (6 \times 10^5 \times \pi)\int_0^\infty N(D)v(D)D^3\,dD$$

($\mathrm{mm\ h^{-1}}$), 7) apparent weather radar rain rate $R_Z = [(1/a)Z)]^{1/b}$ ($\mathrm{mm\ h^{-1}}$), where a and b are empirical constants used in operational weather radar applications, 8) mean fall velocity

$$v_d = \frac{\int_{\mathrm{Nyquist}} v\eta(v)\,dv}{\int_{\mathrm{Nyquist}} \eta(v)\,dv},$$

and 9) peak fall velocity

$$v_e = \frac{\int_{\mathrm{env}} v\eta(v)\,dv}{\int_{\mathrm{env}} \eta(v)\,dv}.$$

TABLE 2. Main system and operating characteristics of the MRR-2.

Wavelength	$\lambda = 1.25$ cm
Transmit power	50 mW
Modulation	FM-CW
Beamwidth (two way, 6 dB)	2°
Antenna	Offset parabola
Radom	No
Range resolution	$\Delta z \geq 10$ m
Lowest analyzed range	$3\Delta z$
No. of range gates	28
Time resolution	$<\Delta t \geq 10$ s
Spectral velocity resolution	$\Delta v = 0.191\ \mathrm{m\ s^{-1}}$
Nyquist velocity range	0–12.3 $\mathrm{m\ s^{-1}}$
No. of power spectra per second	25
Min detectable radar reflectivity ($z = 1000$ m, $\Delta z = 100$ m, $\Delta t = 60$ s)	−2 dBZ

The definition of these parameters and their retrieval procedures are described in more detail in appendix A, which includes also a discussion of the following technical issues: 1) The focus of this paper is the height dependence of microphysical rain parameters. For this application the range-dependent uncertainty of the radar calibration is most critical (whereas the absolute calibration is less relevant). 2) Noise at the radar receiver input would yield a small but continuous apparent rain rate. Therefore, a threshold was introduced to discriminate between rain- and no-rain conditions. 3) At the wavelength of 1.25 cm, attenuation on the path to and from the scattering volume must be taken into account. The particle attenuation is calculated on the basis of the retrieved DSDs, whereas the gas attenuation is neglected. 4) The relation between drop size and fall velocity depends on the air density. Although temporal variations of air density are neglected, its height dependence is considered. 5) The scattering at larger drops cannot be described by Rayleigh scattering, but Mie theory must be employed. 6) In reality the measured Doppler velocity v_m is a composite of the (unknown) vertical wind component w and the terminal fall velocity v: $v_m = v + w$. A mean wind component causes a corresponding shift of the Doppler spectra while unresolved turbulent fluctuations within the scattering volume and within the time resolution of the measurement cause a broadening of the Doppler spectra. The corresponding errors of retrieved DSDs and related parameters are discussed.

3. Strategy of data analysis

The general aim of this study is to reveal vertical mean structures of microphysical rain parameters. We expect that profile structures should depend somehow on the "type" of rain. While various criterions are conceivable to describe the type (e.g., "stratiform" versus "convective" rain), here the rain rate was used as a classification criterion. The class limits and the number of samples falling in each class are given in Table 3.

Some caution is necessary in carrying out this classification, because the instantaneous rain rate shows a large variability with height, such that different portions of the profile might fall in different rain-rate classes.

The striking inhomogeneity of rain fields can be demonstrated with the vertical correlation function defined by

$$C(\zeta) = \frac{\sum_i^N R_i(z_0)R_i(z_0+\zeta) - \frac{1}{N}\sum_i^N R_i(z_0)\sum_i^N R_i(z_0+\zeta)}{\sum_i^N R_i(z_0)^2 - \frac{1}{N}\left[\sum_i^N R_i(z_0)\right]^2}, \quad (1)$$

where i is the sample number and z_0 is some arbitrarily chosen reference height.

Figure 2 shows an example of $C(\zeta)$ representing 1 yr of MRR data from Westermarkelsdorf, Germany (Δz = 35 m), for the reference height $z_0 = 3\Delta z = 105$ m.

The data were stratified according to rain intensities as indicated in Table 3. The half-width $\zeta_{0.5}$ of the correlation function [indicated by the vertical line at $C(\zeta) = 0.5$ in Fig. 2] is particularly small in the lowest and highest rain classes. In the medium classes, containing the bulk of events, the half-width is $\zeta_{0.5} = 5, \ldots, 9\Delta z$. It is noted that $\zeta_{0.5}$—in multiples of Δz—was found to be remarkably independent of Δz (not shown here), which is an indication of scale-free statistics of the rain field.

Therefore, the selection of one "reference" height for the classification would impose a bias on the corresponding mean profiles, particularly for the extreme classes. If, for example, a very low (high) rain rate is found in the reference height, there is an enhanced probability that higher (lower) rain rates are found in other heights.

To avoid this problem, we did not select a particular reference height but we used the profile-averaged rain rate

$$\langle R \rangle = \int_l^u R(z)\, dz/(u-l)$$

for classification.

TABLE 3. Number of samples observed in each rain-rate class from 1 May to 30 Sep in each year. (Many interruptions in Westermarkelsdorf in 2002.)

Classes	Zingst			Westermarkelsdorf		Christiansoe
(mm h^{-1})	2000	2001	2002	2002	2003	2000
0.02–0.2	6344	6725	6496	2779	37 031	3315
0.2–2.0	7319	8467	6960	2793	41 145	6741
2.0–20	1639	2934	3108	793	7692	2044
20–200	186	331	238	26	395	179

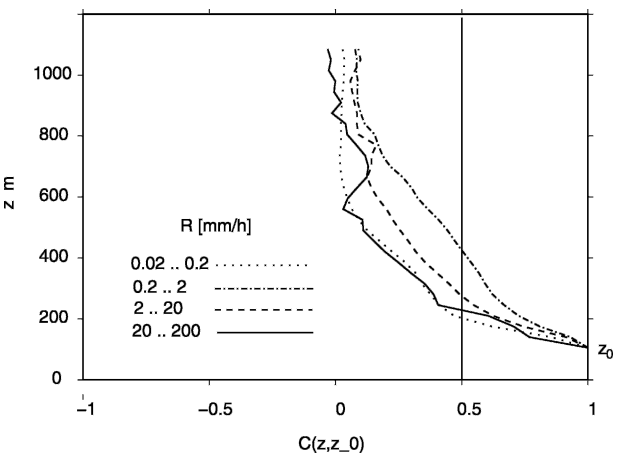

FIG. 2. Correlation function of rain rates in Westermarkelsdorf from 1 May 2003 to 30 Sep 2003.

4. Results

a. Mean profiles of R, LWC, Z_e, and Z

Examples of mean profiles of R, LWC, Z_e, and Z are shown in Fig. 3. The year and site were selected arbitrarily because similar structures were observed generally.

The rain rate (Fig. 3a) is fairly independent of height in the two medium rain classes. In the lowest rain class the negative gradient above 800 m is probably caused by the cloud top. Drizzle is correlated with shallow clouds in this geographic area. The apparent positive R gradient in the highest class is not physically reasonable and may be not real. One potential source of retrieval error for such high rain rates is the overcompensation of attenuation. As is subsequently shown (see Fig. A7 described in appendix A) the estimated mean (two way) attenuation is nearly 4 dB (1500 m)$^{-1}$, which corresponds to about 2 times the observed gradient of R.

The liquid water profiles (Fig. 3b) show an even larger positive gradient in the highest class. While its absolute value is doubtful for the same reasons as in

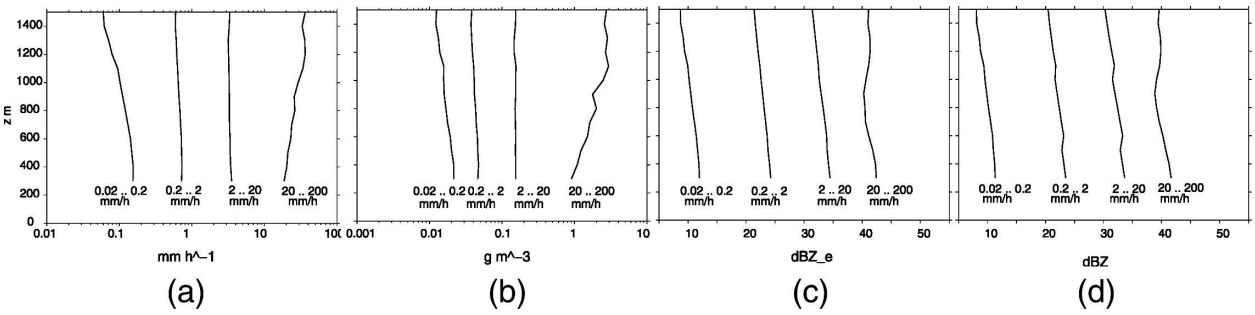

FIG. 3. Profiles of mean rain parameters in Zingst in 2000: (a) rain rate, (b) liquid water content, (c) equivalent radar reflectivity, and (d) radar reflectivity.

case of the rain rate, its difference to the rain-rate gradient is probably real. According to the air density effect (Fig. A8, described in appendix A) the LWC gradient should be smaller than that of the rain-rate gradient for a height-independent DSD shape. We assume that the contrary difference indicates enhanced LWC at higher altitudes caused by a shift of the DSD to smaller drops with a correspondingly lower mass-weighted flux velocity v_m [see appendix A Eq. (A19)].

The radar reflectivities (Figs. 3c and 3d) show negative gradients in all rain-rate classes. In the lowest class the slopes agree with the LWC profile. In all other classes, particularly in the highest class, the slopes disagree. Although the absolute slope may be again unreliable in the highest class, the strong discrepancy between the Z and LWC profiles supports the conjecture that the DSD is shifted toward smaller drops at higher altitudes: because of the D^3 and D^6 proportionality of LWC and Z, respectively, Z decreases for a given LWC, if the drop size is reduced.

Because the mean fall velocities v_d and v_e [see Eqs. (A20) and (A21) for definitions] show the most conspicuous features, they are presented in Fig. 4 for all sites and years that were analyzed. In the highest rain class, v_d decreases significantly with increasing height. [One exception is v_d in Fig. 4e, where only 26 samples corresponding to 260 s were captured in the highest class. Therefore, this outlier may be not significant.]

While near the surface there is fair agreement between the measured fall velocities and the simulations (shown in Fig. A8), the measured and simulated velocity gradients are of the opposite sign. In the simulation height-independent shapes of DSDs were assumed, yielding positive velocity gradients resulting from the air density effect. The observed negative velocity gradients are a further indication of DSD shifts toward smaller drops with increasing height. One might argue that this shift of drop sizes could be a sham caused by a (huge) gradient of (mean) vertical wind that possibly could exist in such strong rain events. A mere shift of the Doppler spectra by vertical wind would nevertheless not explain the systematic difference between the v_d and v_e gradients. The v_d profiles are more tilted than are the v_e profiles. This difference can only be explained by a height-dependent transformation of the shape of the DSDs. The mean power spectra, shown in Fig. 5, provide further support of this conclusion. The spectra stem from the same data as the profiles in Fig. 3. Three heights were selected for presentation, and the spectra were normalized with their peak values. Arithmetic averages are shown in the left row and harmonic averages in the right row, respectively. While the spectral shape is not very height dependent in the lower classes, the enhanced contribution of slower (smaller) drops with increasing altitude is evident in the highest rain-rate class. One could suspect that the enhanced spectral tail at low velocities is just a consequence of enhanced turbulence at higher altitudes. Inspection of the left column shows that the arithmetic mean spectra tend to be broader than their harmonic-mean counterparts. As discussed in appendix B section a, the different widths can be attributed to turbulent broadening, which is only effective in the case of arithmetic averages. One exception is the spectra in the highest class and upper altitudes: the coincident broadening of arithmetic and harmonic averages indicates that the spectral width is not turbulence dominated, but rather is attributed to the broadening of instantaneous spectra.

b. *Z–R relation in different heights*

The benchmark parameter of the quality of weather radar rain estimation is the ratio R/R_Z, which should be height independent and, in the ideal case, equal to unity. Therefore, in Fig. 6 $\overline{R}/\overline{R_Z}$ profiles are shown for all sites and years that were analyzed. The near-surface values of $\overline{R}/\overline{R_Z}$ are generally within the interval of 0.5–2 for all sites and classes (one exception: $\overline{R}/\overline{R_Z} = 3.5$ in Christiansoe, Denmark, for $\overline{R} = 20$–200 mm h^{-1}). This variability could be reduced by adapting the parameters

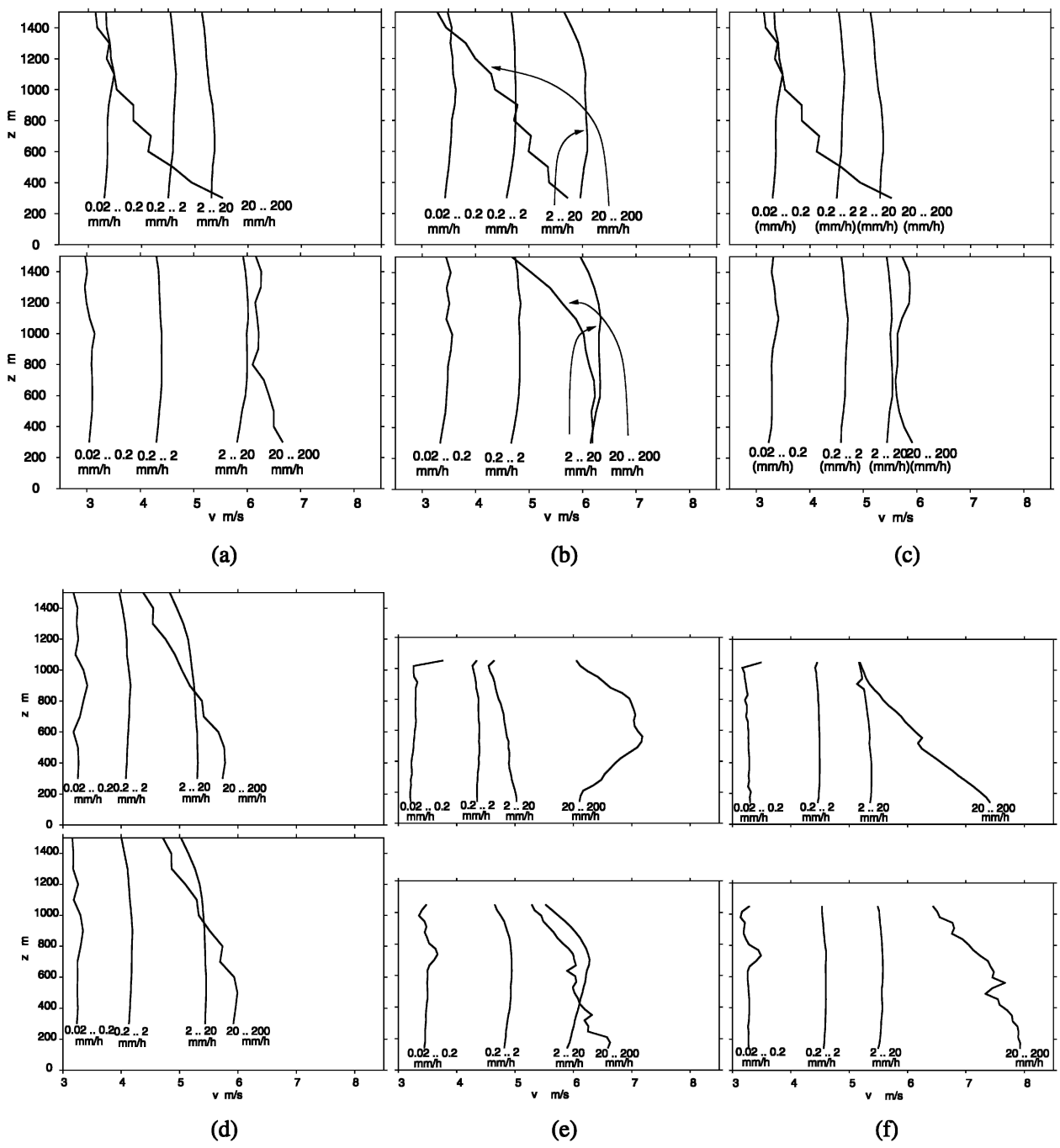

FIG. 4. Profiles of mean fall velocities (top) v_d and (bottom) v_e in (a) Zingst in 2000, (b) Zingst in 2001, (c) Zingst in 2002, (d) Christinansoe in 2000, (e) Westermarkelsdorf in 2002, and (f) Westermarkelsdorf in 2003.

a and b in Eq. (A17) (here $a = 250$ and $b = 1.42$ was used) or by choosing a different functional form of the Z–R relation. This is not the aim of our study, however. More important in this context is the variation of $\overline{R}/\overline{R_Z}$ with height. While this variation is small in the three lower rain classes, the height gradients are significantly positive in the highest rain class in all years and at all sites (e.g., Westermarkelsdorf 2002 is again not significant, because of the small sample size). The corresponding values of $\overline{R}/\overline{R_Z}$ range from 3 to 7 in the highest altitudes (1000–1500 m). These altitudes represent typical lower measuring heights of weather radars, and are usually considered as being relatively reliable heights for rain estimation.

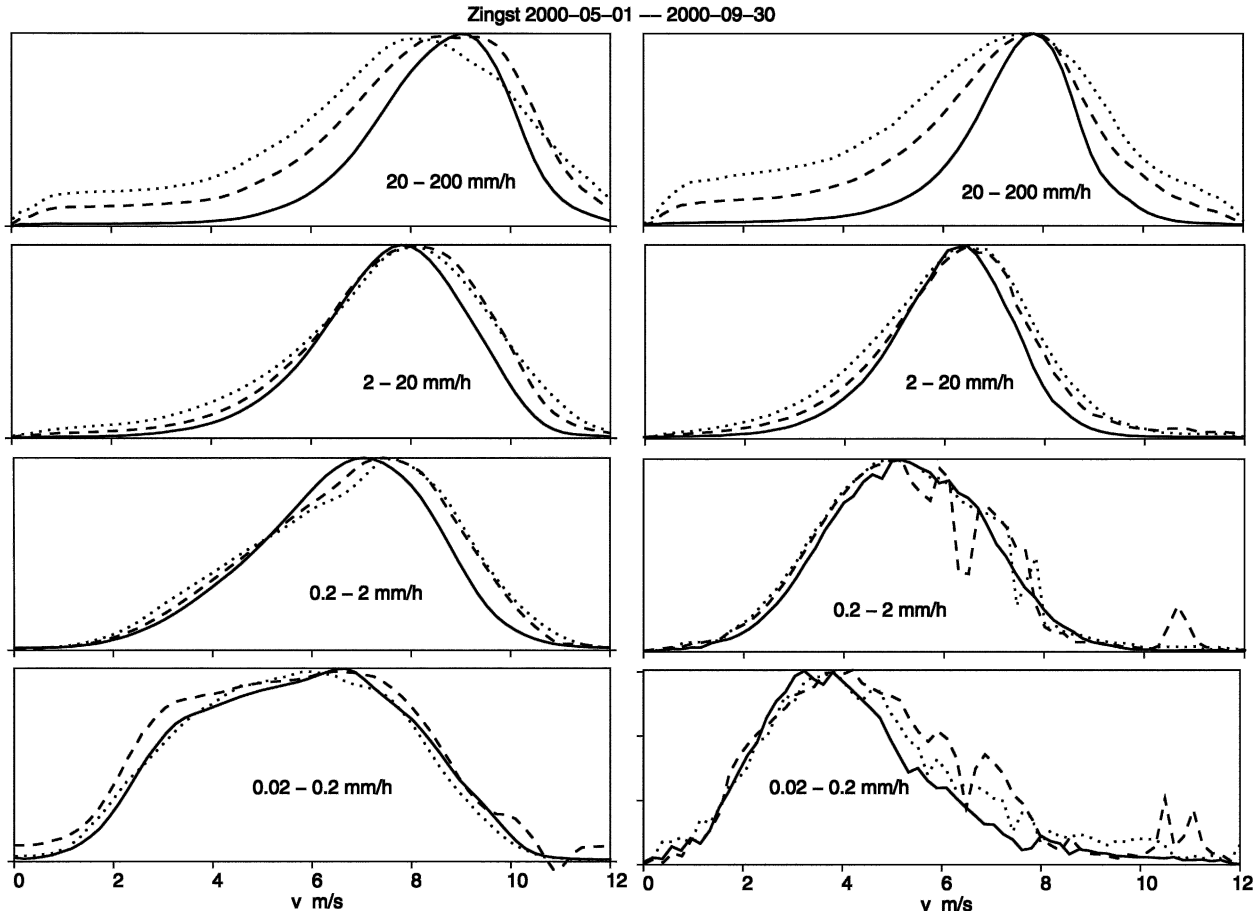

FIG. 5. Mean power spectra in three heights: 300 (solid), 1000 (dashed), and 1500 (dotted) m for the (left) arithmetic average and (right) harmonic average.

The MRR retrievals of Z and R were tentatively used to establish parameter-free Z–R relations for different altitudes using the method described in appendix B section b. An example is shown in Fig. 7. One recognizes good agreement for low and medium rain intensities (representing the bulk of the total rainfall), but at high rain rates the application of the surface-based Z–R relation would yield a systematic underestimation of rain rate.

5. Conclusions

a. Height dependence of DSDs

For weak and medium rain rates, which provide the bulk of the total rainfall at the analyzed measuring sites, Z–R relations are obviously transferable from ground level to lower weather radar measuring heights below the melting level (1–1.5-km altitude in our study).

In case of strong rain rates (>20 mm h^{-1}), on the other hand, a significant height dependence of the shape of DSDs and hence of the Z–R relations was found. Although the contribution to the annual total rainfall may be small, the correct capture of strong rainfall events is most important, for example, for flooding prediction and water management in general. The analysis, based on several years of height-resolved MRR measurements, showed that strong rain events are systematically underestimated by weather radar, if Z–R relations, adapted to surface conditions, are employed. In Zingst, Germany, in 2001 (331 events) and in Westermarkelsdorf in 2003 (395 events) the radar reflectivity decreased by more than a factor of 4 within 1000-m height for given rain rates >20 mm h^{-1}. At other sites and in other years the gradient was less pronounced but still significant.

Although the derivation of height-dependent Z–R relations from MRR data was demonstrated, the application for improved radar rain measurements would require an understanding of the physical process behind the observed height dependences in order to explain

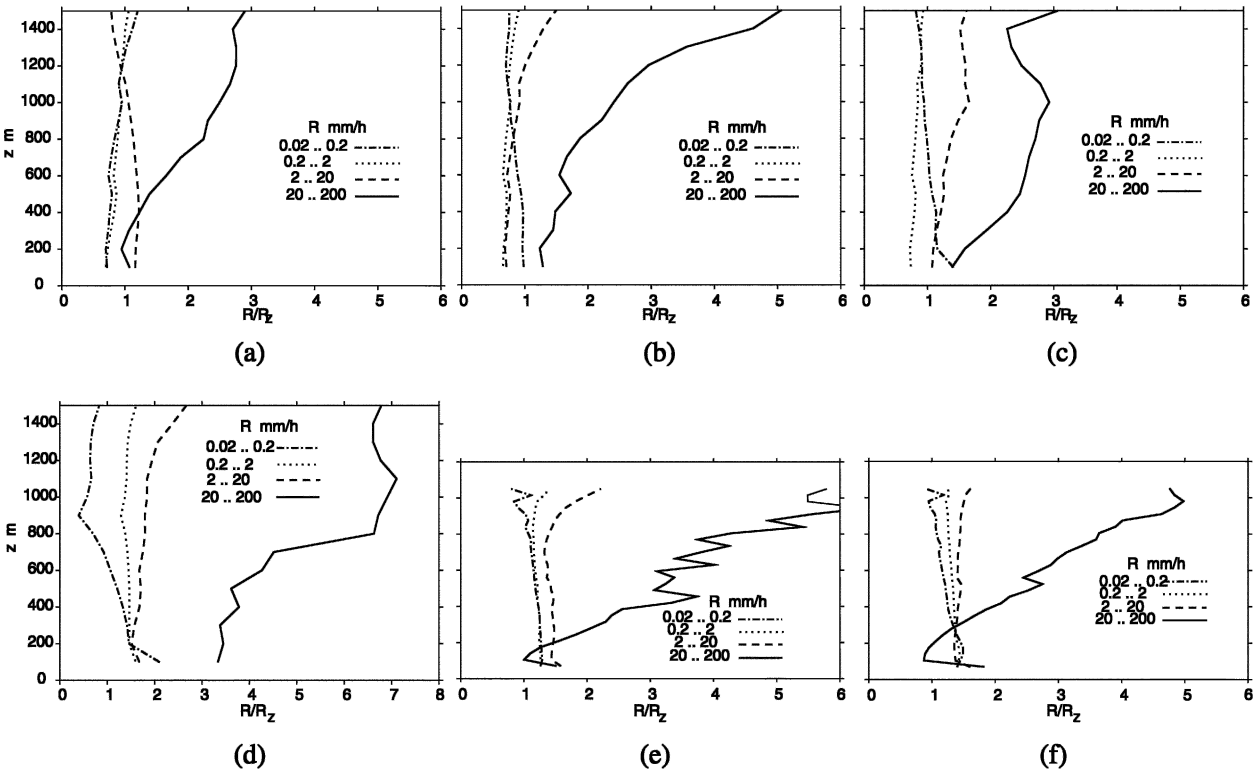

FIG. 6. Profiles of ratio $\overline{R}/\overline{R_Z}$ in (a) Zingst in 2000, (b) Zingst in 2001, (c) Zingst in 2002, (d) Christinansoe in 2000, (e) Westermarkelsdorf in 2002, and (f) Westermarkelsdorf in 2003.

the variability of annual mean profiles between different sites and years. The general tendency—that vertical gradients of DSD parameters are pronounced at high rain rates—is physically reasonable because of the enhanced probability of raindrop collisions, and is in agreement with the theoretical analysis of Hu and Srivastava (1994). However, we are not aware about physically based predictions of the shape of DSDs near the melting level. The variable height of the melting layer may contribute to the variability of the profiles observed in this study. The ongoing analysis of the data will address this question by arranging the vertical axis with respect to the melting level.

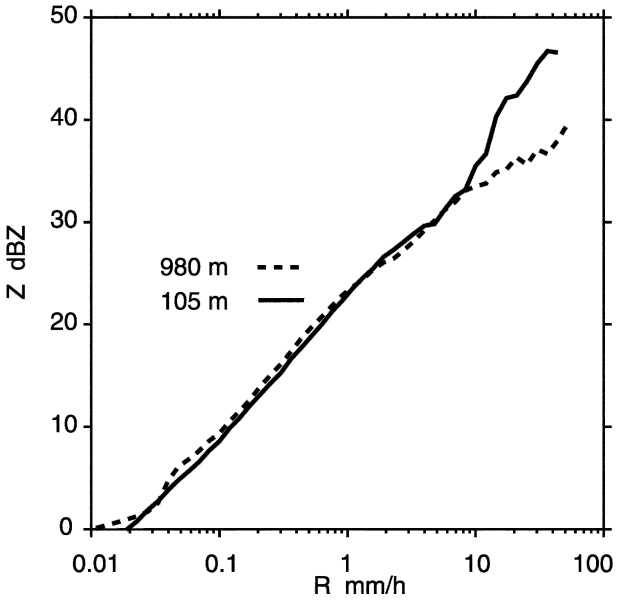

FIG. 7. Westermarkelsdorf mean *Z–R* relations in 2003, derived at 105- and 980-m altitude.

In addition, the employment of other rain classification schemes as "stratiform" and "convective," including features of weather radar reflectivity patterns (e.g., Sempere Torres et al. 2000), may help to improve the prediction of profiles of *Z–R* relations.

b. Reality of nonlinear Z–R relations

Although Jameson and Kostinski (2001b, 2002) cast doubt on the reality of nonlinear *Z–R* relations, we found strong evidence that the shape of the DSDs depends systematically on the rain rate. An obvious indication for the rain-rate dependence of DSDs is the fall velocity v_d, which increases from 3 to 7 m s^{-1} with increasing rain classes and is incidentally in reasonable agreement with the classical Marshall–Palmer parameterization (Fig. A8).

Acknowledgments. The presented work was part of the BMBF-funded project Accurate Areal Precipitation Measurements over Land and Sea (APOLAS) in the frame of the German climate research program DEKLIM. The in situ measurements of vertical wind at a 100-m mast were obtained by the DWD Meteorological Observatory Lindenberg. We thank F. Beyrich and his colleagues for assisting in the experimental setup and for providing the wind data.

APPENDIX A

Retrieval Procedures and Error Analysis

The FM-CW principle implies that the range information is mapped on the frequency axis of the beat signal. Therefore, any frequency dependence of the system gain causes a corresponding range dependence of the received power. Thus, the retrieval of profile structures is ultimately limited by the accuracy of the radar receiver's transfer function $g(f)$. Repeated application of white noise to the receiver input showed that the normalized function $g_n(f) = g(f)/\overline{g(f)}$ was stable within ± 0.05 dB. To obtain the scattering cross section, the usual $1/z^2$ range dependence of the received power was compensated and the rain attenuation was corrected according to an algorithm described in appendix A section a(3). The lowest two range gates ($z < 3\Delta z$) were excluded from the analysis, because several simplifications necessary for a tractable quantitative interpretation of radar signal power do not apply here. Consequently, near-field effects (e.g., deviations from $1/z^2$ range dependence) can be neglected because they fade out at $z \approx 20$ m for this antenna.

Because precipitation takes place only during a small fraction of the total measuring time (typically 5%–10% at this site) a reliable precipitation detection algorithm (PDA) is necessary. Otherwise, noise at the receiver input would lead to a small but continuous artificial precipitation rate during the 95% fraction of time without precipitation causing a significant bias of the total accumulated rainfall. The PDA applied here uses a reference noise spectrum that was measured under controlled conditions without precipitation. If a minimum of five lines of the received spectral power exceeds the reference noise background by 2.6 dB, precipitation is detected in the corresponding range gate. This leads to the detection threshold for Z as indicated in Table 2. Because of this procedure the false-alarm rate increases with increasing measuring height and with decreasing averaging time, but it is negligible at least below 1500-m height for 10-s averages.

a. DSD retrieval

1) Drop size distributions

The basic equation to derive DSDs from the Doppler spectra is

$$N(D, z)\Delta D = \frac{\eta(D, z)}{\sigma(D)}\Delta D, \tag{A1}$$

where $N(D, z)$ is the spectral drop number density (dimension m^{-4}) at the measuring height z, and $\eta(D, z)$ is the spectral volume scattering cross section as function of the drop diameter D. It is related to $\eta(v, z)$ in the Doppler velocity domain via the derivative of Eq. (A5),

$$\eta(D, z) = \eta(v, z)\left[\frac{\partial D(v, z)}{\partial v}\right], \tag{A2}$$

where $\eta(v, z)$ is obtained from the measured Doppler spectrum $p_r(v, z)$ by applying the radar equation

$$\eta(v, z) = \frac{C_R}{g_n(z)} z^2 l(z) p_r(v, z), \tag{A3}$$

where C_R is a constant containing radar parameters as transmit power, antenna and receiver gain, and line losses, which have to be determined once by calibration; $g_n(z)$ is the normalized transfer function, where the frequency f was replaced with range z using $z = (f/f_s)|_t c/2B$; f_s is the sweep frequency of the frequency modulation, $|_t$ is the truncation operator yielding the next lower natural number (applies for down sweep), c is the velocity of light, B is the modulation bandwidth, and $l(z)$ is the attenuation on the two-way propagation path. Its estimation is explained in appendix A section a(3).

The single particle backscattering cross section that is calculated with Mie theory is $\sigma(D)$ using the code of Morrison and Cross (1974). The diameter D is defined as the diameter of a sphere with the droplet volume V [$D \equiv (V \times 6/\pi)^{(1/3)}$]. The cross section relative to the Rayleigh approximation is shown as a function of diameter in Fig. A1.

For parameters like liquid water or rain rate it is useful to convert the Doppler spectrum into a function of (sphere equivalent) drop diameter D. This parameter is not immediately available but must be inferred from the Doppler velocity v. Under the (restrictive) assumption of zero vertical wind, v can be identified with the terminal fall velocity. For the conversion of v into D we use the analytic fit of Atlas et al. (1973) to the data of Gunn and Kinzer (1949).

$$D(v) = \frac{1}{0.6}\ln\frac{10.3}{9.65 - v}. \tag{A4}$$

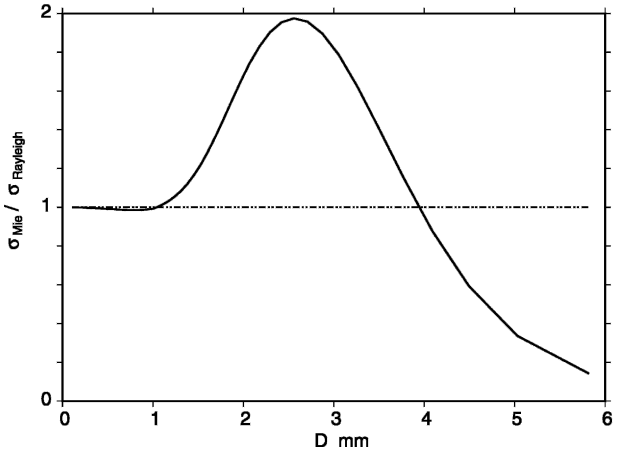

FIG. A1. Single particle scattering cross section of droplets divided by the Rayleigh approximation.

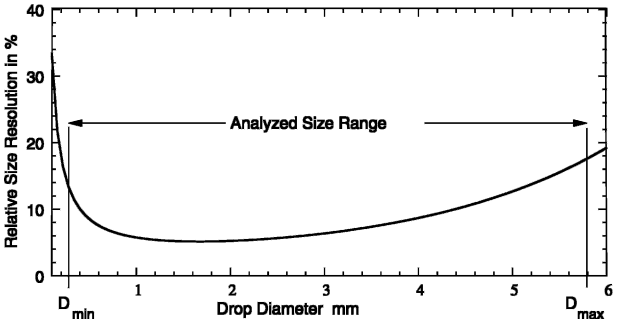

FIG. A2. Relative drop size resolution $\Delta D/D$ vs D for a fixed velocity resolution $\Delta v = 0.191$ m s^{-1} and analyzed diameter range assuming liquid phase.

where $D(v)$ is in millimeters and v is in meters per second. Equation (A4) is applicable for $|v| < 9.62$ m s^{-1} corresponding to $D < 5.8$ mm (spherical mass equivalent) drop diameter. Larger drops are unstable and contribute generally only very little to the liquid water content (LWC) or rain rate R (although larger velocities may occur in the ice phase or for partly melted hydrometeors). We nevertheless limited the analyzed size range to $D \leq 5.8$ mm (corresponding to $v = 9.36$ m s^{-1}) to keep clear from the pole of Eq. (A4) at $v = 9.65$ m s^{-1}.

In addition, a lower limit was introduced for the analyzed range, in order to avoid instabilities, explained in the following: Eq. (A1) shows that $N(D) \propto \eta(D)/\sigma(D)$. Because η is a measured value, it shows some noisy deviation s from the "true value" η_t. So we may rewrite $N(D) = [\eta_t(D) + s]/\sigma(D) = N(D)_t + s/\sigma(D)$. For small drops the Rayleigh approximation $\eta \propto N(D)\, D^6$ and $\sigma \propto D^6$ holds, which yields $N(D)_t - N(D) = s/D^6$. The stochastic error s/D^6 of $N(D)$ goes rapidly to ∞ as D approaches zero. The corresponding relations for spectral liquid water content and rain rate [$\mathrm{LWC}(D)_t - \mathrm{LWC}(D) \propto s/D^3$ and $R(D)_t - R(D) \propto s/D^2$] are less dramatic in the small drop regime, but the vicinity of $D = 0$ must be avoided as well. Equation (A4) is applicable anyway only for drop sizes $D > 0.11$ mm. (At this diameter the equation would deliver a zero fall speed.) Therefore, the lower limit of the analyzed range was set to $D_{\min} = 0.246$ mm corresponding to $v_{\min} = 0.76$ m s^{-1}, assuming that smaller drops may be neglected for rainfall estimation. (This neglect is of course not applicable to cloud LWC, because this parameter is, in contrast with rain rate, dominated by drops with $D < D_{\min}$).

Because of the nonlinearity of Eq. (A4) the bin width ΔD is not constant but is a function of D (see Fig. A2).

Equation (A4) and thus the limits $D_{\min}$ and $D_{\max}$ are strictly valid only for a certain air density ρ. While weather-related temporal variations of ρ are neglected, the height dependence of air density is taken into account by adopting a generalized form of Eq. (A4):

$$D(v, z) = \frac{1}{0.6} \ln \frac{10.3}{9.65 - v/\delta_v(z)}. \tag{A5}$$

Using the $v \propto \rho^{-0.4}$ dependence found by Foote and du Toit (1969) and assuming *U.S. Standard Atmosphere, 1976* conditions the height-dependent correction of v can be approximated by a second-order polynomial,

$$\delta(z) = (1 + 3.68 \times 10^{-5} z + 1.71 \times 10^{-9} z^2), \tag{A6}$$

where z is the height above sea level.

We assume that the range of validity of Eq. (A6) is the same as that of Eq. (A4) after replacing v by $v/\delta_v(z)$. The corresponding height dependence of the analyzed velocity range is shown in Fig. A3 for $\Delta z = 100$ m. The sawtooth shape of $D_{\max}$ is a result of the finite frequency resolution of the Fourier transform. The upper half of this profile is not of concern for our data because it is (in moderate climate zones) often above the melting level, where Eq. (A4) is not applicable anyway.

2) COMPARISON WITH IN SITU DISDROMETER MEASUREMENTS

The radar data obtained at the lowest reliable altitude (100 m in Westermarkeldorf and 300 m in Zingst) were compared with surface in situ measurements of DSDs in order to validate the retrieval method described in the previous section. The classical "Joss–Waldvogel" disdrometer ("JW") as well as an optical disdrometer (OD) developed by Großklaus et al. (1998) was used for comparison. Figure A4 shows the

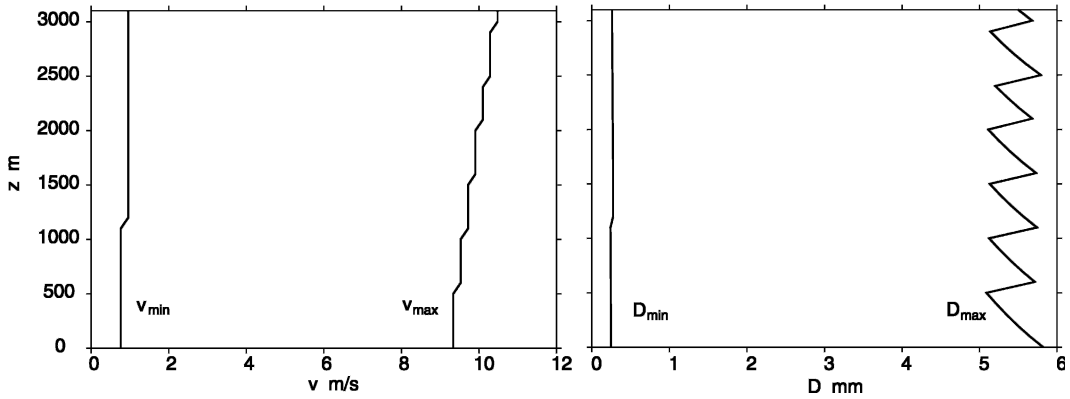

FIG. A3. Analyzed (left) velocity and (right) diameter range as a function of height.

comparison of time series during a 5-h rain event measured in Westermarkelsdorf in April 2003. The rain rates (top) and the median droplet diameter (bottom) show excellent agreement. An overview of mean DSDs as obtained in Zingst during 2003 is shown in Fig. A5. The DSDs were classified according to three ranges of rain rate corresponding to Figs. A5a, A5b, and A5c. The number of samples is indicated by *S*. Each sample

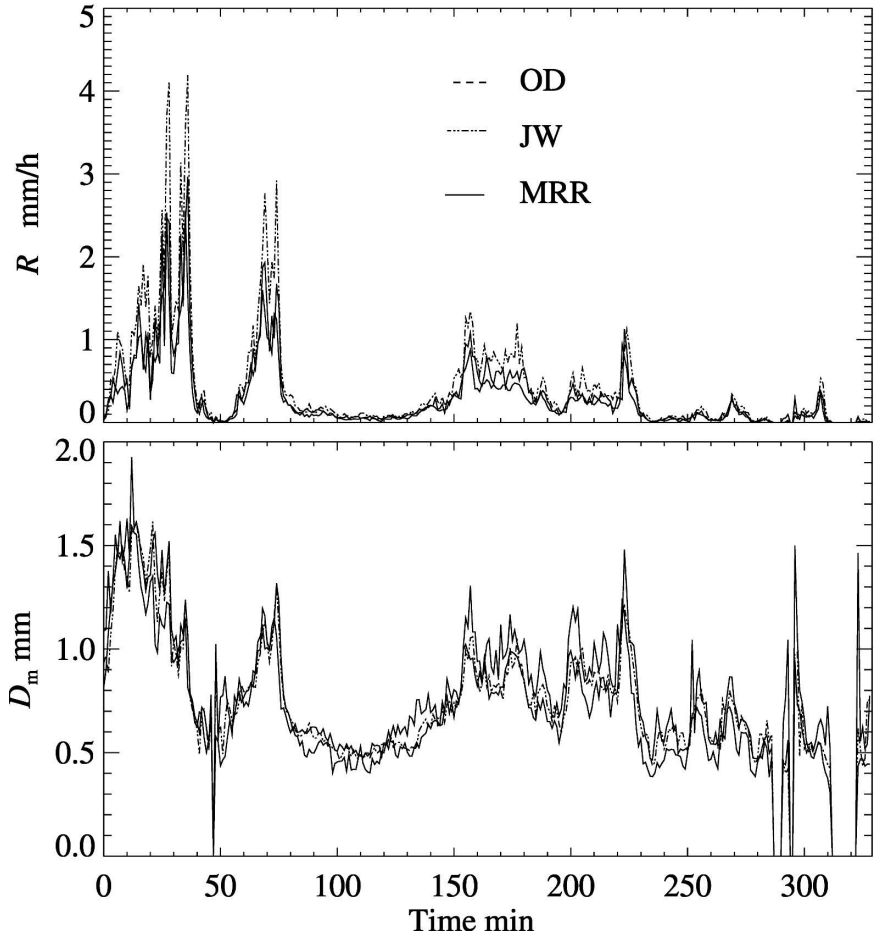

FIG. A4. Comparison between MRR and two different in situ disdrometers. Time series of rain event 13 in Westermarkelsdorf in Apr 2003: (top) rain rate and (bottom) median drop diameter.

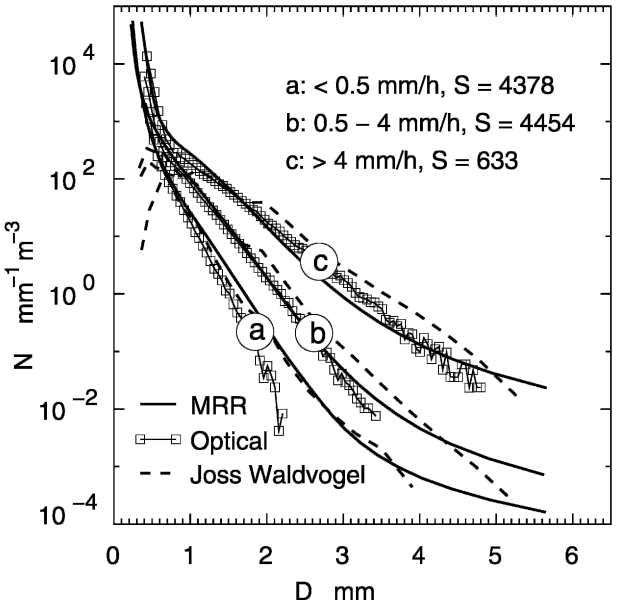

FIG. A5. Comparison between MRR and two different in situ disdrometers. Mean drop size distributions in Zingst in 2003: S = number of samples. Each sample represents 1 min.

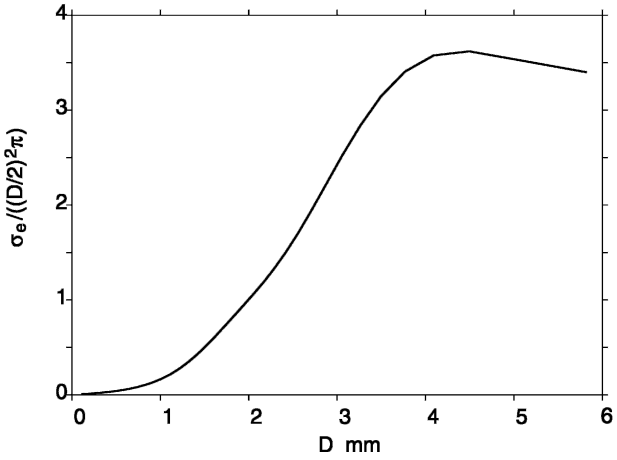

FIG. A6. Normalized single particle extinction cross section σ_e vs D.

represents a 1-min average. While there is reasonable agreement around 1-mm drop diameter, one recognizes major deviations of the JW DSDs for small drops and moderate deviations in the larger diameter region between all three sensors. An in-depth discussion of these comparisons is beyond the scope of this paper, but we may summarize that the deviations of the MRR DSDs from the in situ DSDs are in the same range as the mutual deviations of the in situ DSDs.

3) ATTENUATION CORRECTION

Basically two contributions to the attenuation must be considered—the gaseous absorption κ_g and the rain extinction κ_r. The gaseous absorption coefficient is governed by the absolute humidity ρ_h and is, for sea level conditions ($\rho_h = 7.5$ g m^{-3}, $p = 1013$ hPa, $T = 300$ K), $\kappa_g = 0.18$ dB km^{-1} (Ulaby et al. 1981). The mean κ_g on a vertical beam should be generally smaller than this value, because of decreasing ρ_h with increasing z. We decided to neglect κ_g because we restrict here the quantitative interpretation of the radar reflectivity for other reasons anyway to $z \leq 1500$ m of the atmosphere. The rain attenuation on the other hand is taken into account by applying a recursive algorithm developed by Kunz (1998). The single particle extinction cross section $\sigma_e(D)$ normalized with the geometric cross section was calculated by Mie scattering theory (Fig. A6).

In the lowest range gate all spectral and integral parameters $p(z_1)$, which are proportional to the received power [e.g., $\eta(v, z_1)$, $\eta(D, z_1)$, $N(D, z_1)$, Z_e, and Z] are derived neglecting attenuation [$l(z_1) = 1$] in Eq. (A3). The rain attenuation coefficient $\kappa_r(z_1)$ is calculated by $N(D)$-weighted integration of $\sigma_e(D)$ over D,

$$\kappa_r(z_1) = \int_{D_{\min}}^{D_{\max}} \sigma_e(D) N(D, z_1)\, dD. \tag{A7}$$

The attenuation, caused by the first range gate, and thus effective in the second range gate, is estimated according to

$$l(z_2) = \exp[-2\kappa_r(z_1)\Delta z], \tag{A8}$$

with Δz range resolution. (The factor of 2 accounts for the two-way propagation.) The attenuation-corrected parameters $p(z_2)_{\text{cor}}$, including $N(D, z_2)_{\text{cor}}$, are obtained by

$$p(z_2)_{\text{cor}} = \frac{p(z_2)_{\text{raw}}}{l(z_1)}; \tag{A9}$$

$N(D, z_2)_{\text{cor}}$ is then used to estimate the attenuation exerted by the second range gate. This allows us to calculate the attenuation-corrected parameters in range gate 3, and so on. This procedure is only stable as long as the total two-way path attenuation does not exceed a certain limit (≈5 dB in our experience). If there is any range gate i with $2\kappa_r(z_i)\Delta z > 1.4$, data for higher range gates are flagged as being invalid. Figure A7 shows mean attenuation profiles for four classes of rain rates, with each class spanning one decade of rain rates. The linear mean

$$\langle l_{\text{rain-class}}(z) \rangle = \frac{1}{N_{\text{rain-class}}} \sum_{i \in \text{rain-class}}^{N_{\text{rain-class}}} l_i \tag{A10}$$

was calculated for data obtained from 1 May 2000 to 30

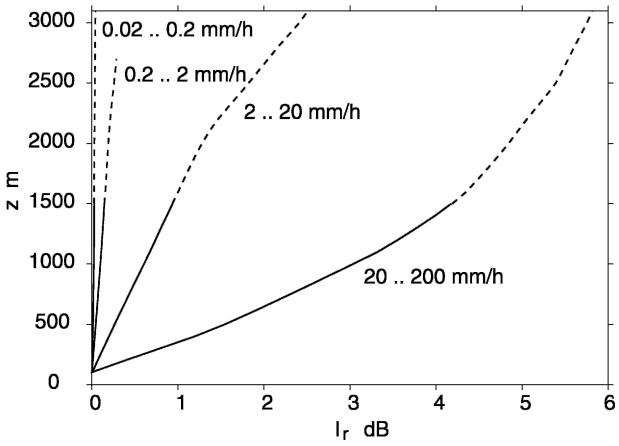

FIG. A7. Profiles of two-way rain attenuation l_r as obtained by repeated application of Eqs. (A7), (A8), and (A9) for four rain-rate classes. Data are from Zingst from 1 May 2000 to 30 Sep 2000. The solid lines cover the liquid-phase height range.

September 2000. The mean structure is pretty similar in the years 2001 and 2002 (not shown here). All heights were treated as if they contain solely liquid phase precipitation, which is realistic only below 1500 m (solid lines) because the melting layer sank down to this level occasionally (with 6% probability).

b. Integral DSD parameters

1) RADAR REFLECTIVITY FACTORS Z AND Z_E

The radar reflectivity factor Z is defined as the sixth moment of the DSD:

$$Z = \int_0^\infty N(D)D^6\,dD, \tag{A11}$$

where Z is the most common parameter for radar-based rainfall estimation, because it is simply proportional to the received echo power in the Rayleigh-scattering regime. Because weather radars operate in this regime, Z is obtained directly from the weather radar volume backscatter cross section η_{wr} by division through a constant A, which contains physical parameters of the scattering process [wavelength, complex refractive index of water (ice), shape of the hydrometeors; see e.g., Doviak and Zrnic (1993)],

$$Z = \eta/A \quad \text{for} \quad D \ll \lambda. \tag{A12}$$

MRRs operate at shorter wavelengths, where the Rayleigh approximation does not hold in the entire size range. Nevertheless, one can calculate the expression η/A, but it is no longer the sixth moment of the DSD. Therefore, this parameter is commonly referred to as equivalent radar reflectivity factor Z_e,

$$Z_e = \eta/A \quad \text{for} \quad D \text{ not} \ll \lambda. \tag{A13}$$

In contrast to Z, Z_e depends on the radar wavelength.

To facilitate comparisons between MRRs and weather radars, Z is derived from MRR DSDs using Eq. (A14),

$$Z = \int_{D_{\min}}^{D_{\max}} N(D)D^6\,dD, \tag{A14}$$

which is identical with Eq. (A11), except for the integration limits, which embrace the analyzed size range introduced in appendix A section a(1).

2) LIQUID WATER CONTENT LWC AND RAIN RATE R

These parameters are obtained by appropriately weighted integration of the DSD:

$$\mathrm{LWC} = \rho_w \frac{\pi}{6} \int_{D_{\min}}^{D_{\max}} N(D)D^3\,dD \tag{A15}$$

and

$$R = \frac{\pi}{6} \int_{D_{\min}}^{D_{\max}} N(D)v(D)D^3\,dD. \tag{A16}$$

3) Z-BASED RAIN RATE R_Z

The derivation of rain rate, as described in appendix A section b(2), is based on actually measured spectra and does not depend on the assumption of certain shapes of DSDs. It is therefore instructive to compare the rain rate, derived with Eq. (A16), with rain rates, as obtained with some Z–R relation. The deviation between R and R_Z is an immediate measure for the quality of the considered Z–R relation. A widely used empirical form is

$$Z = aR^b, \tag{A17}$$

where Z has units of millimeters to the sixth power divided by millimeters cubed, R has units of millimeters per hour, and a and b adopt specific values depending on climatic conditions and on the radar calibration database .

We define R_Z (mm h^{-1}) accordingly:

$$R_Z = \left(\frac{Z}{a}\right)^{1/b}. \tag{A18}$$

The conclusions drawn in this study do not depend sensitively on the quality and hence not on the actual choice of the parameters a and b because not the deviation between R and R_Z itself but rather the height dependence of this deviation is considered.

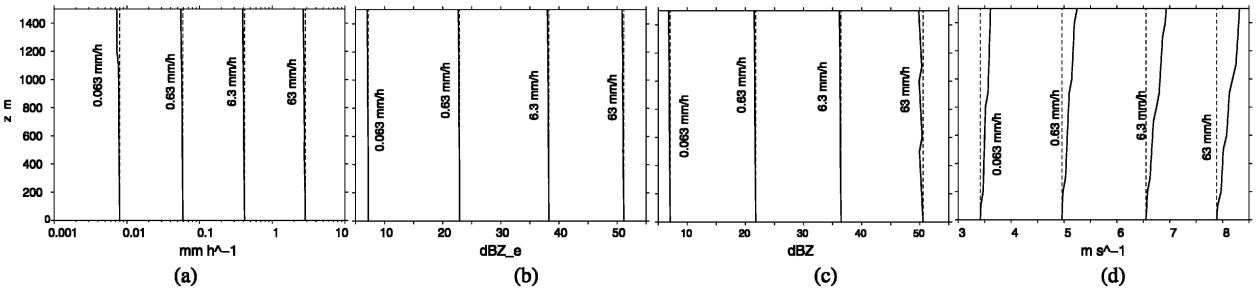

FIG. A8. Simulated profiles of various parameters assuming constant flux (solid lines). Vertical auxiliary lines (dashed lines), coinciding with the parameters at $z = 0$; (a) liquid water content, (b) equivalent radar reflectivity factor, (c) radar reflectivity factor, and (d) mean fall velocity v_d.

4) MEAN FALL VELOCITIES

Various definitions of the mean fall velocity are possible. One useful definition is the mass-weighted velocity v_l representing the mean mass-flux velocity because it is equal to the ratio of rain rate to liquid water content

$$v_l = R/\mathrm{LWC}. \tag{A19}$$

Because v_l does not contain new information in addition to R and LWC it is not shown explicitly.

Another widely used definition of fall velocity is the $\eta(v)$-weighted mean velocity, that is, the first moment of the Doppler spectrum, which is commonly referred to as the mean Doppler velocity. It emphasizes the larger drops' velocities resulting from the D dependence of the single particle scattering cross section ($\propto D^6$ in the Rayleigh regime),

$$v_d = \frac{\int_{\mathrm{Nyquist}} v\eta(v)\, dv}{\int_{\mathrm{Nyquist}} \eta(v)\, dv}. \tag{A20}$$

The integration is extended over the full Nyquist velocity range of the radar, which is 12.3 m s^{-1} for the MRR.

Further, the velocity of the peak of the Doppler spectrum can be considered. Because the peak position might not be well defined, particularly in the case of broad peaks, a more stable estimate is obtained by calculating a truncated first moment with integration limits in the neighborhood of the peak, for example,

$$v_e(z) = \frac{\int_{\mathrm{env}} \eta(v, z)v\, dv}{\int_{\mathrm{env}} \eta(v, z)\, dv}, \tag{A21}$$

where the environment env of the spectral peak $\eta_{\max}$ is limited by v_{upper} and v_{lower}, which are given by the conditions $\eta(v_{\mathrm{upper}}) = \eta(v_{\mathrm{lower}}) = \eta_{\max}/e$.

In case of symmetric spectra v_d and v_e agree, whereas differences between v_d and v_e reveal asymmetric structures in the tails of the Doppler spectra.

c. The effect of air density

The effect of air density on the vertical fall velocity was already described in Eq. (A6). Here we show the consequences of the air density gradient for the profiles of radar reflectivity, liquid water content, and the mean fall velocity v_d under the assumption of height-independent flux and height-independent shape of MP drop-size distributions. For this purpose simulated Doppler spectra were calculated on the basis of MP DSDs corresponding to the (harmonic) mean rain rate of the respective rain class, taking into account the vertical air density gradient assuming *U.S. Standard Atmosphere, 1976*. These Doppler spectra were processed exactly in the same way as measured spectra, including truncation of the Doppler spectra at velocities corresponding to drop diameters of 0.25 and 5.8 mm, respectively. The results are presented in Fig. A8. We recognize for all parameters except v_d a slightly negative gradient, as is to be expected according to the air density profile. The step structure showing up in some of the profiles is because of the finite line width and the height-dependent truncation of the MRR spectra.

d. The effect of mean vertical wind and turbulence

1) OVERVIEW

Equation (A5), which relates the drop size to the fall velocity, is valid only in stagnant air. Unfortunately, radar signals obtained at K band in precipitation do not contain independent information on the wind field. Although various schemes to estimate the vertical wind from K-band precipitation spectra were suggested (e.g., Rogers 1964; Hauser and Amayenc 1983), the quality of

TABLE A1. Vertical wind errors for various integral parameters and estimated range of corresponding vertical gradients.

P	LEM [dB $(\mathrm{m\,s^{-1}})^{-1}$]	∇_{LEM} (dB $\mathrm{km^{-1}}$)	LET [dB $(\mathrm{m^2\,s^{-2}})^{-1}$]	∇_{LET} (dB $\mathrm{km^{-1}}$)
R	3.4	$\pm$0.34	1.4	$-$0.3
LWC	4.3	$\pm$0.43	2.1	$-$0.4
κ_R	3.0	$\pm$0.3	0.8	$-$0.2
Z_e	$-$2	$\mp$0.2	$-$1.3	0.3
Z	1	$\pm$0.1	$\pm$1.3	$\mp$0.3
R_Z/R	$-$3.8	$\mp$0.38	$-$1.7	+0.3

these schemes has not yet been assessed. Application of these schemes and comparisons with vertical wind measurements on a nearby tower (not shown here) indicated that the estimation error could be much larger than the actual vertical wind. Consequently, vertical wind "corrections" may even deteriorate the quality of rain parameter estimates, at least in low- or medium-turbulence conditions. Therefore, zero vertical wind was assumed for this study, and the impact of this assumption on the accuracy of all considered integral parameters was estimated. The quantitative sensitivity to vertical wind does not only depend on the shape of the actual DSD but also on the choice of the limits of the analyzed spectral range. The truncation of spectra at fixed velocities, as applied in the MRR signal analysis [see section a(1)], can aggravate or mitigate the wind error.

Logarithmic normalized relative mean errors LEM_P and LET_P are introduced to describe the effect of mean vertical wind and of the variance of its turbulent fluctuations, respectively,

$$\mathrm{LEM}_P \equiv \frac{1}{w}\,10\log\left(\frac{P_w}{P_{w=0}}\right) \tag{A22}$$

and

$$\mathrm{LET}_P \equiv \frac{1}{\sigma_w^2}\,10\log\left(\frac{P_{\sigma\_w}}{P_{w=0}}\right), \tag{A23}$$

where P_w is the estimated value of parameter P for vertical wind speed w, and P_{σ_w} is the estimated value of parameter P for zero mean turbulence with the variance σ_w^2.

As shown in appendix A sections d(2) and d(3), LEM_P and LET_p are about constants for realistic values of w and σ_w^2 with characteristic values for each parameter P.

In this context, it is not these values themselves but rather than their expected height gradients that are of concern. Their w-related uncertainty was estimated by multiplying the normalized errors with a realistic range of gradients of w and σ_w^2, respectively,

$$\nabla_{\mathrm{LEM}} = \mathrm{LEM}\nabla(w) \quad \text{and} \quad \nabla_{\mathrm{LET}} = \mathrm{LET}\nabla(\sigma_w^2).$$

As a first approximation a linear height dependence is assumed, and the mean gradient is estimated for a height range of 1 km.

We assume that a mean gradient of w within $\pm$0.1 m $\mathrm{s^{-1}}$ $\mathrm{km^{-1}}$ is a conservative estimate. Similarly, we assume that the mean gradient of σ_w^2 is within $\nabla(\sigma_w^2) = \pm 0.2$ $\mathrm{m^2\,s^{-2}\,km^{-1}}$. The last estimate is supported by long-term turbulence measurements in the lower few hundred meters of the atmosphere at a location with comparable climatic and orographic conditions of the radar sites. Mean values of $\sigma_w^2 = 0.2$ $\mathrm{m^2\,s^{-2}}$ with a standard deviation of $\mathrm{std}(\sigma_w^2) = 0.2$ $\mathrm{m^2\,s^{-2}}$ (Peters and Fischer 2002) were found for near-neutral conditions. In case that the turbulence dies out at 1.5-km altitude the mean gradient would assume $\nabla(\sigma_w^2) = -0.2$ $\mathrm{m^2\,s^{-2}\,km^{-1}}$.

A summary of the effects of mean vertical wind and of turbulence together with the estimated ranges of mean vertical gradients is given in Table A1.

The vertical wind error was simulated by calculating the parameters P assuming Marshall–Palmer DSDs,

$$N_{\mathrm{mp}}(D) = N_0 e^{-\Lambda D}, \tag{A24}$$

which are related to the rain rate via $\Lambda = 4.1R_{\mathrm{mp}}^{-0.21}$, where Λ has units of inverse millimeters and the R term is in millimeters per hour. The index mp shall be a reminder of the fact that R_{mp} is neither identical with R, obtained with Eq. (A16), nor with R_z, obtained with Eq. (A18). Sempere Torres et al. (1994) already analytically showed that R, R_{mp}, and R_Z cannot be mutually reconciled. To minimize this internal inconsistency of common parameterizations, the parameters a and b in Eq. (A17) were fitted for the least squares difference between R_Z and R_{mp} in the range $0.01 < R_{\mathrm{mp}} < 1000$ mm $\mathrm{h^{-1}}$. The fit, $a = 250$ and $b = 1.42$, is in the range of usually adopted Z–R relations and was used throughout this study.

2) MEAN VERTICAL WIND

The Marshall–Palmer DSDs of Eq. (A24) were transformed into Doppler spectra by inversion of Eqs. (A1), (A2), and (A4), and the resulting Doppler spectra were shifted in five steps by full line widths between -0.76 and + 0.76 m $\mathrm{s^{-1}}$ to simulate the mean vertical wind w. (The positive sign stands for upwind.)

From the shifted spectra (while keeping the truncation limits v_{min} and v_{max} fixed at the values used by the MRR for $z = 0$, see Fig. A3) the biased DSDs and various integral parameters, including rain rate R and the ratio R_Z/R, were calculated according to the scheme described in appendix A section a.

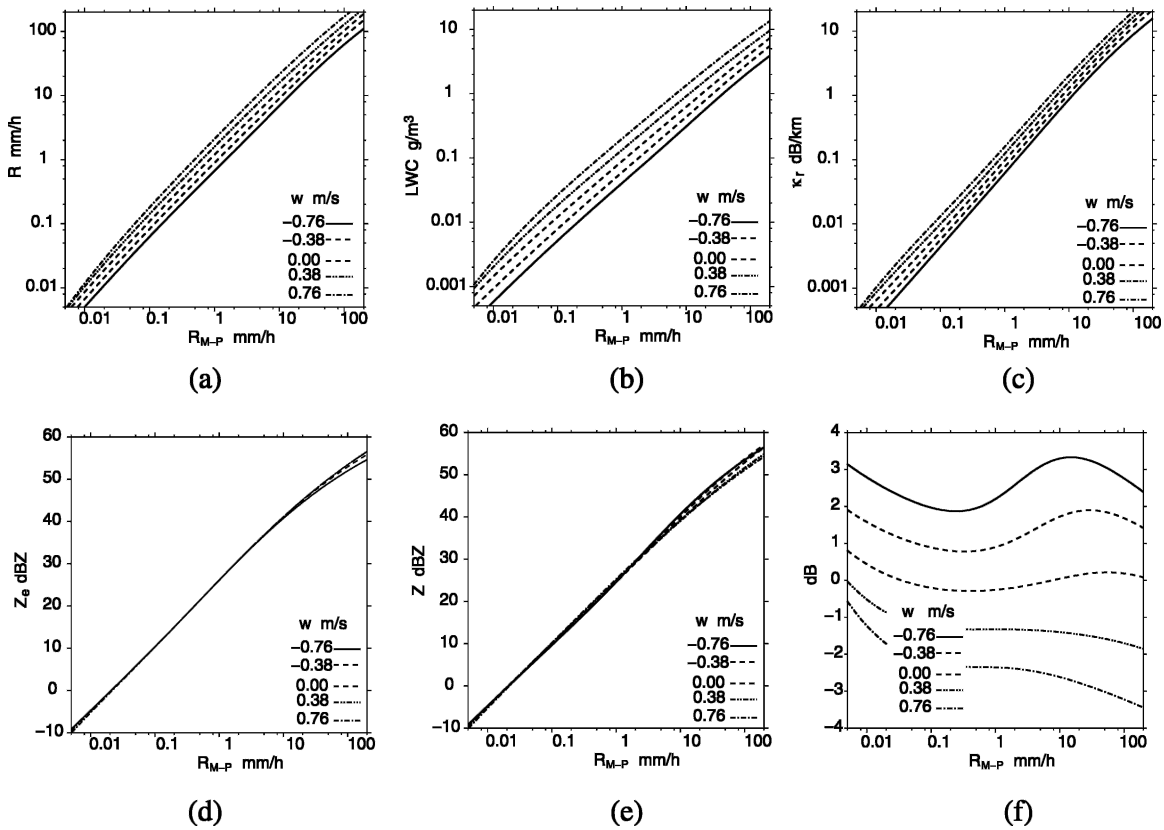

FIG. A9. Simulated rain parameters vs Marshall–Palmer rain rate for different values of vertical wind in the range ± 0.76 m s^{-1} (positive sign = upwind); (a) rain rate, (b) liquid water, (c) attenuation coefficient, (d) equivalent radar reflectivity, (e) radar reflectivity, and (f) $R_Z/R = (Z/250)^{1/1.42}/R$.

The results are shown in Fig. A9a–f. The logarithmic errors of R, LWC, and κ_r are fairly linear with w in the presented range of w, and they are nearly independent of R_{mp} in a wide range of rain rates (Fig. A9a–c). This justifies the introduction of the mean logarithmic normalized errors, shown in Table A1. The rain attenuation coefficient κ_r is of concern only at higher rain rates ($\approx$1 dB km^{-1} at $R = 10$ mm h^{-1}). Consequently, also its wind error $\mathrm{LEM}_\kappa \approx 3$ dB (m s^{-1})$^{-1}$ matters only at rain rates higher than 10 mm h^{-1}. The radar reflectivities Z_e and Z show nearly no sensitivity to vertical wind at moderate rain rates (Fig. A9d–e). Some small deviations occur at rain rates $>$10 mm h^{-1}. Downwind causes the Doppler velocities of large drops to exceed the integration limit v_{max} leading to an underestimation of Z_e. In case of Z an additional error takes effect, which overcompensates the truncation error: The shift of retrieved drop sizes causes an erroneous transformation of Mie to Rayleigh scattering cross sections of larger drops. The cross-sensitivity of R_Z/R to w decides if the gradients of R_Z/R are dominated by height-dependent DSDs (a problem of weather radars) or height-dependent vertical wind (a problem of MRRs; Fig. A9f). If the parameterizations, relating R, R_Z, and R_{mp}, would be self-consistent, R_Z/R should be unity for $w = 0$. The parameters a and b in Eq. (A17) were not fitted for this goal rather than for $R_Z/R_{\mathrm{mp}} \rightarrow 1$. Thus, the mean value of R_Z/R shows some mean deviation from unity and some wavelike dependence on the rain rate. For the purpose of this study these deviations are of no concern, when compared with retrieval errors of the vertical gradient of R_Z/R. For a conservative estimate, shown in Table A1, we used the highest sensitivity of R_Z/R to w, $\mathrm{LEM}_{R_Z/R} \approx -3.8$ dB (m s^{-1})$^{-1}$, occurring at rain rates $>$10 mm h^{-1}.

In addition to these simulations, which hinge on the validity of Marshall–Palmer DSDs, real data, obtained on the test site "Falkenberg" of the German Weather Service (52°10′N, 14°07′E), were also examined. For this purpose a MRR was operated for 5 months close to an ultrasonic anemometer, mounted on top of a 100-m tower in 40-m horizontal distance. The range resolution of the MRR was set to 10 m, and the 10th range gate, centered at 100-m height, was compared with the sonic

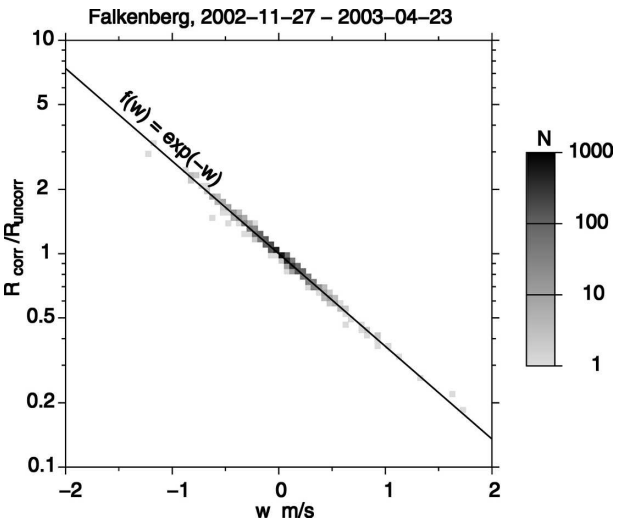

FIG. A10. Regression of $R_{\text{corr}}/R_{\text{uncorr}}$ vs w.

anemometer. The MRR as well as the sonic anemometer data were averaged over 1-min intervals, and the vertical wind from the sonic anemometer was used to remove the wind shift of the Doppler spectra in order to retrieve corrected rain rates. Although the horizontal distance between MRR and the sonic anemometer prevents a perfect correction, we believe that this procedure provides a realistic estimate of the cross sensitivity of retrieved rain rates to the vertical wind. Figure A10 shows the ratio of corrected and uncorrected rain rate $R_{\text{corr}}/R_{\text{uncorr}}$ on a logarithmic scale. In agreement with the simulations, the dependence of the logarithmic ratio on w is amazingly linear. [The constant of proportionality happens to be unity, if the natural logarithm and International System of Units (SI) units are used.] This constant corresponds to $\text{LEM}_R = 4.3$ dB $(\text{m s}^{-1})^{-1}$, which is slightly more than the simulation value in Table A1 [3.4 dB $(\text{m s}^{-1})^{-1}$].

3) TURBULENCE WITH ZERO MEAN

Zero mean wind fluctuations can have nonzero mean effects on the rain parameters for the following two reasons: 1) correlation between the rain rate and vertical wind, and 2) nonlinear dependence of the retrieval error on vertical wind. It is still an open question, whether or not significant correlation exists between the rain rate and the vertical wind component. Positive correlation, attributed to convection-triggered rain, and negative correlation, caused by friction-induced downdrafts, are physically plausible. Simultaneous measurements of both parameters w and R were reported by Richter (1994), but too few rain events were analyzed to allow for general conclusions. In the above-mentioned Falkenberg data no significant correlation was found. Other simultaneous measurements of hydrometeors and air motion with UHF and VHF radar wind profilers (e.g., Wakasugi et al. 1986) or measurements using the Lhermitte method (Lhermitte 1988; Kollias et al. 1999) were to our knowledge not analyzed with respect to this issue. We assume for the following that there is no general correlation between R and w, bearing in mind that verification of this assumption is needed. Without correlation one is left with the nonlinear dependence of the estimated parameter P on w causing a residual mean error as described by Eq. (A23).

A rough estimate of this effect is obtained by assuming a binary distribution of w, hopping between w_h and $-w_h$. In this case one obtains $\overline{\Delta P} = 0.5(P_{w=+w_h} + P_{w=-w_h}) - P_{w=0}$. The corresponding standard deviation of w is $\sigma_w = w_h$. For the choice of w_h one must keep in mind that too small values will not show nonlinear effects. High values, on the other hand, lead to effects that may occur in individual cases but do not represent typical atmospheric conditions. The following results are based on $w_h = \sigma_w = 0.76$ m s^{-1}, corresponding to the range of four spectral lines of the MRR Fourier transform.

The results are shown in Fig. A11. Similar as for the mean wind in Fig. A9, Z_e and Z show nearly no sensitivity to w except for very high high rain rates. Because the w sensitivity of all parameters depend on R_{mp}, the maximum values were picked for a conservative estimate; κ_R deviations were considered again only for $R_{\text{mp}} > 10$ mm h^{-1}. The corresponding normalized errors LET_P, shown in Table A1, are the approximate bias proportional to the variance σ_w^2.

APPENDIX B

Potential Pitfalls in Averaging Rain Data

a. Averaging of spectra and rain parameters

Mean rain parameters can be obtained in many different ways, which are generally not equivalent. For example, mean rain parameters could be derived from mean power spectra. Alternatively, rain parameters, derived from instantaneous spectra, could be averaged in order to get their mean values. There is a continuum of choices between these extremes, with some partitioning of averaging of spectra and of rain parameters. We decided to (online) average the spectra over periods of 6 or 56 s, respectively, mainly in order to keep the data volume manageable. The corresponding measurement repetition periods are 10 and 60 s (see Table 1), which include 4-s data transfer time in addition to

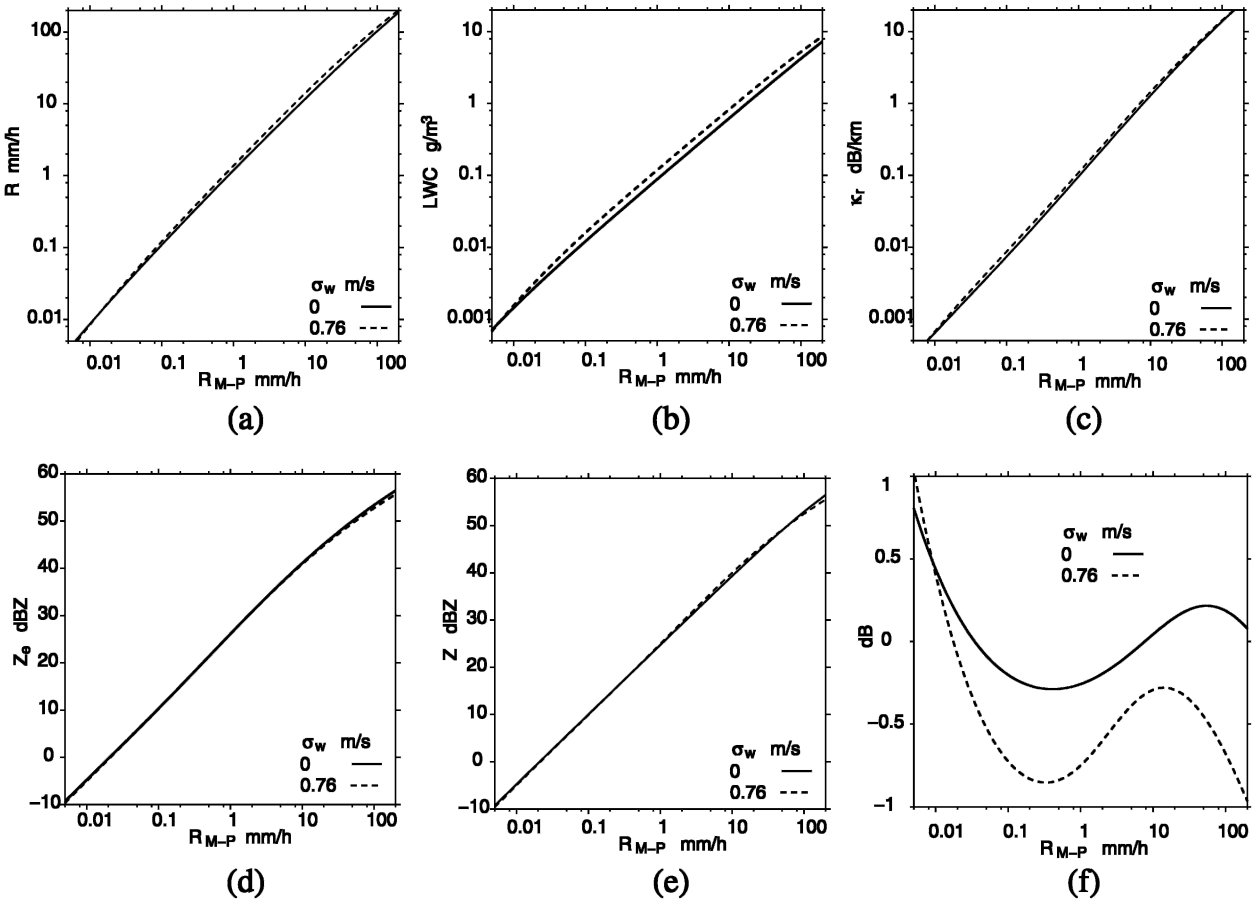

FIG. A11. Simulated rain parameters vs Marshall–Palmer rain rate for different levels of turbulence: zero turbulence (solid lines) and vertical wind hopping between 0.76 and -0.76 m s^{-1} (dashed lines); (a) rain rate, (b) liquid water, (c) attenuation coefficient, (d) equivalent radar reflectivity, (e) radar reflectivity, and (f) $R_Z/R = (Z/250)^{1/1.42}/R$.

the net averaging time. The corresponding numbers of power spectra in each averaging period are 150 and 1400. The remaining averaging (over summer seasons) in each rain-rate class was performed on the rain parameter level.

There is a further choice concerning averaging: widely used alternatives are arithmetic or harmonic averages. The fall speeds v_d and v_e show normal distributions. In this case the arithmetic mean is a natural choice. We preferred to calculate also arithmetic averages for R, LWC, Z_e, Z, and Z_R, although the lognormal shape of their probability density functions (PDFs) would suggest harmonic averages. The reason is the ill behavior of harmonic averages of sets containing zeroes or negative values. Spurious zeroes and negative values may occur, because the parameters are retrieved from spectra after subtraction of an estimated noise level.

While the profiles of R_Z and R depend on the profiles of total drop number densities and on possibly imperfect treatments of attenuation or of the radar transfer function, the ratio R/R_Z should be less sensitive to these effects because they appear in the nominator and denominator. Therefore, the profiles of the mean ratio $\overline{R}/\overline{R_Z}$ are used as indicator for systematic changes of the DSD shape and hence of the Z–R relation with height.

b. Mean Z–R relations

The regressions of Z versus R, as obtained from the DSDs, were condensed to mean Z–R relations. Because there exists at present no theoretical argument for a certain functional form of Z–R relations, we did not follow the usual procedure that fits some predefined function (typically of the form $Z = aR^b$) with only a few free parameters to the data. The large amount of data allows for a different analysis with less restrictive assumptions: rain-rate classes of 0.8-dB class width (i.e., $10 \log \delta R/R = 0.8$) were formed, and for each class i the corresponding radar reflectivities were averaged arithmetically, yielding the relation $\overline{Z_i}(R_i)$ with $R_i = R_0 \times 10^{i0.08}$. In this procedure R is the independent variable.

The result was shown in Fig. 7. It is of course also possible to form classes Z_i and to choose Z as an independent variable. This would be the right choice for weather radar application, where the resulting function $\overline{R_i}(Z_i)$ serves to derive R from measurements of Z. Because the correlation of Z and R is high, $\overline{R_i}(Z_i)$ does not differ much from the inverse function $R_i(\overline{Z_i})$ (not shown here).

APPENDIX C

Width and Energy of Mean Doppler Spectra from Rain in Turbulence

The interpretation of mean power spectra suffers mainly from one ambiguity: the width of the mean spectra is determined by the convolution of two distributions, namely the power spectrum in stagnant air $p_r(v)$ and the PDF of vertical wind $p_w(v)$. Remarkably, the relative contributions of these effects to the spectral width depend on the kind of averaging, which offers a possibility to separate these contributions. In case of a Gaussian from $p_r(v)$, arithmetic mean spectra are broadened by turbulence while their energy is conserved, and harmonic mean spectra are *not* broadened by turbulence while their energy is reduced. Because the real spectral forms may deviate considerably from Gaussian shape, we do not claim that the width of the harmonic mean spectra is totally insensitive to turbulence. Nevertheless, we believe that the comparison of arithmetic and harmonic averages of spectra provides hints on the significance of turbulence contributions to the spectral width.

We consider a set of identical rain spectra, which are assumed to be Gaussian for simplicity, and are described in stagnant air by

$$p_r(v) = \exp(-v^2), \tag{C1}$$

where the velocity v is nondimensionalized using the spectral width σ_r (i.e., $v/\sqrt{2}\sigma_r \rightarrow v$).

The effect of vertical wind is described by a corresponding shift of v,

$$p_r(v) = \exp[-(v - w)^2]. \tag{C2}$$

[We do not consider broadening of individual spectra $p_r(v)$ by nonresolved turbulence.]

a. Arithmetic average

The arithmetic average is obtained by

$$\overline{p_r(v)} = \int_{-\infty}^{\infty} \exp[-(v - w)^2]p(w)\, dw, \tag{C3}$$

where $p(w)$ is the PDF of the turbulent vertical wind component. Equation (C3) represents a convolution and causes a corresponding broadening of $\overline{p_r(v)}$. Because of

$$\int_{-\infty}^{\infty} p(w)\, dw = 1$$

the condition

$$\int_{-\infty}^{\infty} p_r(v)\, dv = \int_{-\infty}^{\infty} \overline{p_r(v)}\, dv \tag{C4}$$

is satisfied, that is, the energy is conserved. For a Gaussian turbulent velocity distribution $p_w(v)$ the width of $\overline{p_r(v)}$ is easily calculated with the well-known result

$$\overline{\sigma_r} = (\sigma_r^2 + \sigma_w^2)^{0.5}, \tag{C5}$$

where σ_w^2 is the variance of the vertical wind component.

b. Harmonic average

The harmonic average of $p_r(v)$ can be obtained by the following steps: 1)take the logarithm of the spectra, 2) calculate the arithmetic average, and 3) take the exponential.

In analogy with Eq. (C3) we obtain for the harmonic average

$$\begin{aligned}\widehat{p_r(v)} &= \exp\left(\int_{-\infty}^{\infty} \ln\{\exp[-(v - w)^2]\}p(w)\, dw\right)\\ &= \exp\left[-\int_{-\infty}^{\infty} (v - w)^2 p(w)\, dw\right]\\ &= \exp\left[\underbrace{-v^2\int_{-\infty}^{\infty} p(w)\, dw}_{=1} + \underbrace{2v\int_{-\infty}^{\infty} wp(w)\, dw}_{=0} - \underbrace{\int_{-\infty}^{\infty} w^2 p(w)\, dw}_{=\sigma_w^2}\right].\end{aligned} \tag{C6}$$

One recognizes that $\widehat{p_r(v)}$ is a Gaussian function with the same width as $p_r(v)$, QED.

The energy of $\widehat{p_r(v)}$ is reduced by $a = \exp(-\sigma_w^2)$ or, after undoing the nondimensionalization of the velocity, (i.e., $w \rightarrow w/\sqrt{2}\sigma_r$): $a = \exp(-\sigma_w^2/(2\sigma_r^2))$.

REFERENCES

Atlas, D., R. Srivastava, and R. Sekhon, 1973: Doppler radar characteristics of precipitation at vertical incidence. *Rev. Geophys. Space Phys.,* **11,** 1–35.

Doviak, R. J., and D. S. Zrnic, 1993: *Doppler Radar and Weather Observations*. Academic Press, 562 pp.

Einfalt, T., K. Arnbjerg-Nielsen, C. Golz, N. E. Jensen, M. Quirmbach, G. Vaes, and B. Vieux, 2004: Towards a roadmap for use of radar rainfall data in urban drainage. *J. Hydrol.,* **299,** 186–202.

Foote, G. B., and P. S. du Toit, 1969: Terminal velocity of rain drops aloft. *J. Appl. Meteor.,* **8,** 249–253.

Großklaus, M., K. Uhlig, and L. Hasse, 1998: An optical disdrometer for use in high wind speeds. *J. Atmos. Oceanic Technol.,* **15,** 1051–1059.

Gunn, R., and G. D. Kinzer, 1949: The terminal velocity of fall for water droplets in stagnant air. *J. Meteor.,* **6,** 243–248.

Hauser, D., and P. Amayenc, 1983: Exponential size distribution of raindrops and vertical air motions deduced from vertically pointing radar data using a new method. *J. Climate Appl. Meteor.,* **22,** 407–418.

Jameson, A. R., and A. B. Kostinski, 2001a: What is a raindrop size distribution? *Bull. Amer. Meteor. Soc.,* **82,** 1169–1176.

——, and ——, 2001b: Reconsideration of the physical and empirical origins of *Z*-*R*-Relations in radar meteorology. *Quart. J. Roy. Meteor. Soc.,* **127,** 517–538.

——, and ——, 2002: Spurious power law relations among rainfall and radar parameters. *Quart. J. Roy. Meteor. Soc.,* **128,** 2045–2058.

Hu, Z., and R. C. Srivastava, 1995: Evolution of raindrop size distribution by coalescence, breakup, and evaporation: Theory and observations. *J. Atmos. Sci.,* **52,** 1761–1783.

Koistinen, J., and D. B. Michelson, 2002: BALTEX weather radar-based precipitation products and their accuracies. *Bor. Environ. Res.,* **7,** 253–263.

Kollias, P., R. Lhermitte, and B. A. Albrecht, 1999: Vertical air motion and raindrop size distributions in convective systems using 94 GHz radar. *Geophys. Res. Lett.,* **26,** 3109–3112.

Kunz, M., 1998: Niederschlagsmessungen mit einem vertikal ausgerichteten K-Band FM-CW-Dopplerradar. Diplomarbeit (Diploma thesis), Institut für Meteorologie und Klimaforschung, Universität Karlsruhe, 95 pp.

Lhermitte, R., 1988: Observations of rain at vertical incidence with a 94 GHz Doppler radar: An insight of Mie scattering. *Geophys. Res. Lett.,* **15,** 1125–1128.

Morrison, J. A., and M. J. Cross, 1974: Scattering of a plane electromagnetic wave by axisymmetric raindrops. *Bell Syst. Tech. J.,* **53,** 955–1019.

Peters, G., and B. Fischer, 2002: Parameterization of wind and turbulence profiles in the atmospheric boundary layer based on sodar and sonic measurements. *Meteor. Z.,* **11,** 255–266.

——, ——, and T. Andersson, 2002: Rain observations with a vertically looking Micro Rain Radar (MRR). *Bor. Environ. Res.,* **7,** 353–362.

Richter, M. C., 1994: Niederschlagsmessungen mit dem vertikal ausgerichteten FM-CW-Dopplerradar-RASS-System. Ph.D. thesis, Berichte aus dem Zentrum für Meeres und Klimaforschung, Reihe A: Meteorologie, 12, 143 pp.

Rogers, R. R., 1964: An extension of the *Z*–*R* relationship for Doppler radar. *Proc. 1964 World Conf. on Radio Meteorology and 11th Weather Radar Conf.,* Amer. Meteor. Soc., 158–169.

Sempere Torres, D., J. M. Porra, and J. D. Creutin, 1994: A general formulation for raindrop size distribution. *J. Appl. Meteor.,* **33,** 1494–1502.

——, R. Sanchez-Diezma, I. Zawadzki, and J. D. Creutin, 2000: Identification of stratiform and convective areas using radar data with application to the improvement of DSD analysis and Z-R relations. *Phys. Chem. Earth,* **25,** 985–990.

Strauch, R., 1971: Theory and application of the FM-CW Doppler radar. Dissertation, Colorado University, 97 pp.

Ulaby, F. T., R. K. Moore, and A. K. Fung, 1981: *Microwave Remote Sensing I*. Addison-Wesley, 456 pp.

Wagner, A., J. Seltmann, M. Diederich, and G. Peters, 2003: Coupling a vertically looking K-band radar and a C-band weather radar to obtain a complete profile of reflectivity. *Geophys. Res. Abstracts,* **5,** 11 993.

Wakasugi, K., A. Mizutani, M. Matsuo, S. Fukao, and S. Kato, 1986: A direct method for deriving drop-size distributions and vertical air motions from VHF Doppler radar spectra. *J. Atmos. Oceanic Technol.,* **3,** 623–629.